Wet spinning of strong cellulosic fibres with incorporation of phase change material capsules stabilized by cellulose nanocrystals

Carbohydrate Polymers 312 (2023) 120734

Contents lists available at ScienceDirect

Carbohydrate Polymers

journal homepage: www.elsevier.com/locate/carbpol

Wet spinning of strong cellulosic fibres with incorporation of phase change material capsules stabilized by cellulose nanocrystals

Archana Samanta [a,1], Oleksandr Nechyporchuk [b], Romain Bordes [a,*]

[a] Department of Chemistry and Chemical Engineering, Applied Chemistry, Chalmers University of Technology, 412 96 Gothenburg, Sweden
[b] RISE - Research Institutes of Sweden, Box 104, Mölndal 431 22, Sweden

ARTICLE INFO

Keywords:
Phase change material
Nano-cellulose
Wet spinning
Pickering emulsion
Microsphere
Fibre

ABSTRACT

Incorporating a phase change material (PCM) into fibres allows the fabrication of smart textiles with thermo-regulating properties. Previously, such fibres have been made from thermoplastic polymers, usually petroleum-based and non-biodegradable, or from regenerated cellulose, such as viscose. Herein, strong fibres are developed from aqueous dispersions of nano-cellulose and dispersed microspheres with phase changing characteristics using a wet spinning technique employing a pH shift approach. Good distribution of the microspheres and proper compatibility with the cellulosic matrix was demonstrated by formulating the wax as a Pickering emulsion using cellulose nanocrystals (CNC) as stabilizing particles. The wax was subsequently incorporated into a dispersion of cellulose nanofibrils, the latter being responsible for the mechanical strength of the spun fibres. It was possible to produce fibres highly loaded with the microspheres (40 wt%) with a tenacity of 13 cN tex^{-1} (135 MPa). The fibres possessed good thermo-regulating features by absorbing and releasing heat without undergoing structural changes, while maintaining the PCM domain sizes intact. Finally, good washing fastness and PCM leak resistance were demonstrated, making the fibres suitable for thermo-regulative applications. Continuous fabrication of bio-based fibres with entrapped PCMs may find applications as reinforcements in composites or hybrid filaments.

1. Introduction

For passive thermal regulation, phase change materials (PCM) constitute one of the most straightforward approaches discovered and exploited in applications where energy storage capability is central (Aftab et al., 2018; Li et al., 2017; Sharma et al., 2009; Zhou et al., 2012). Their unique feature of good latent heat storage enables high energy storage density with minimal variation of volume over temperature changes (Song et al., 2021).

One of the earliest marking examples of the use of PCM is related to the space exploration programme Apollo, where wax was employed to maintain the temperature of the batteries of the Lunar Roving Vehicle between 5 and 50 °C (Ferreira et al., 2010). Since then, PCM have found applications in textiles, packaging, and construction materials (Cui et al., 2017; Revaiah et al., 2019; Singh et al., 2018).

PCM has also been incorporated in various matrices including thin films, composites, mortar, concrete, plasterboards and other to feature thermo-regulating properties (Barako et al., 2018; Cunha et al., 2016; Ling & Poon, 2013; Lotnyk et al., 2019; McLaggan et al., 2018). Prior to matrix incorporation, PCM are typically encapsulated through emulsion polymerization where the shell material is polymerized, thereby protecting the PCM core (Zhao et al., 2020). The protecting shell with a defined thickness protects PCM and prevents leakage. Different techniques are reported for fabricating PCM capsules, such as interfacial and in-situ polymerization, composite coagulation, self-assembly and sol-gel processes (Deveci & Basal, 2009; Li et al., 2018; Sarier et al., 2015; Wei et al., 2013; Yu et al., 2014). Alternatively, PCM can be dispersed in the form of an emulsion to be further processed (Zheng et al., 2022). For this purpose, Pickering emulsions have received considerable attention lately since particle-stabilized emulsions that are solidified into beads are normally more stable compared to surfactants-based. Furthermore, surfactants may also leach out (Bahsi Kaya et al., 2022). These beads can be regarded as microspheres that can then be dispersed into a matrix to form a composite (Shi et al., 2021). The colloidal stability of the formulation and the interfacial properties between the microspheres and the matrix polymer play a crucial role in determining the properties of

* Corresponding author.
E-mail address: bordes@chalmers.se (R. Bordes).
[1] Present address: Department of Applied Physics, KTH Royal Institute of Technology, Stockholm 114 19, Sweden.

https://doi.org/10.1016/j.carbpol.2023.120734
Received 17 October 2022; Received in revised form 16 February 2023; Accepted 19 February 2023
Available online 23 February 2023

the final composite as the aggregation of microspheres can prevent its uniform distribution, whereas poor interfacial adhesion between microspheres and the matrix may lead to leakage of the PCM. In the end both aspects negatively impact the properties of the composite.

Among the various forms of composites where PCM microcapsules and microspheres have been introduced, fibres with high aspect ratios have attracted increasing attention, primarily because of their versatility of applications, such as reinforcing agents, crystallinity and interfacial adhesion boosters in composites, special grade yarns, textiles and others (Bledzki, 1999; Dhanabalan et al., 2019; Prajapati & Kandasubramanian, 2019; Zhang et al., 2013). Research on PCM incorporation into fibre technology has been conducted to provide an improved thermal protection for high-end textiles (Mondal, 2008; Revaiah et al., 2019). PCM can be embedded into fabrics using techniques such as coating, padding or lamination (Iqbal et al., 2019; Meng et al., 2015; Paulo et al., 2019; Yang et al., 2010; Zhou et al., 2015). Introduction of the PCM capsules can also be done at the spinning stage, provided that they can resist the high shear forces exerted during the process. It has been so far restricted to synthetic fibres that are predominantly petroleum-based and non-biodegradable (Iqbal et al., 2019). The possible integration of PCM into rayon-like fibres, e.g. viscose which is produced via a process of cellulose xanthation using carbon disulfide that is a reprotoxic chemical causing major environmental issues, has also been reported (Cimilli Duru et al., 2019). This approach, compared to deposition of PCM capsules onto the surface of the substrate, prevents PCM loss via abrasion and washing.

In the field of fibre spinning, nano-cellulose has recently gained considerable attention, allowing using water-based dispersions of bio-based cellulose nanofibres and mild coagulation media to produce the fibres (Clemons, 2016; Lundahl et al., 2017), while taking advantages of the outstanding properties of nanocellulose (Azizi Samir et al., 2005; Habibi et al., 2010; Nechyporchuk et al., 2016; Saito et al., 2013; Siró & Plackett, 2010). Various approaches including wet, dry or dry-jet wet, and microfluidic spinning have been adopted for fibre spinning from CNF (Hooshmand et al., 2015; Iwamoto et al., 2011; Lundahl et al., 2016; Mertaniemi et al., 2016; Nechyporchuk et al., 2018; Shen et al., 2016; Vuoriluoto et al., 2017; Walther et al., 2011). However, reports on fabrication of fibres from CNF containing functional additives, that may hinder the spinning process as well as the final fibre properties, are quite scarce. In this context the introduction of PCM to form thermoregulatory CNF-based fibres can offer the possibility to broaden the use of cellulose-based man-made fibres. It also underpins several challenges starting with the compatibility of the PCM and the cellulose-based matrix. Here, we hypothesize that a PCM microspheres based on paraffin wax (PW) prepared through Pickering emulsion using cellulose nanocrystals (CNC) as stabilizer (Capron et al., 2017) could facilitate the integration of PCM in the cellulose matrix as well as the wet-spinning process. The concept of using CNC as a stabilizing agent for Pickering emulsion of PCM is further acclaimed to minimize the leaching effect which might have occurred in case of an organic surfactant. Further, the use of CNC to prepare the microcapsules is expected to limit the loss of mechanical properties of the resultant fibres by acting as reinforcing agent.

2. Hypothesis

Cellulose based materials are looked upon as ecofriendly substitutes over synthetic fossil fuel-based products. Development of functional cellulosic fibre is an interesting domain which can greatly reduce the dependency on synthetic polymer systems of nylon and polyester for fabrication of textile fibres. Production of stimuli responsive thermoregulatory textile fibres using phase change materials (PCM) can apt to change in external conditions and provide comfort to the wearer. However, it is easier to disperse commercially available hydrophobic PCM into synthetic polymer systems. Direct entrapment of commonly used PCM into cellulose matrix is challenging and creates dope instabilities because of poor dispersibility and compatibility. It is hypothesized that encapsulation of hydrophobic PCM using under the form of droplet stabilized by cellulose nanocrystals (CNC) can solve this issue as CNC will be of similar nature as the matrix. These droplets of PCMs covered with CNC can then be dispersed into cellulose nanofibril (CNF) matrix to produce a dope. Extrusion of the CNF dope containing CNC-PCM capsules can result in fabrication of continuous filaments. Entrapment of the CNC-PCM capsules is expected to provide excellent leak resistance capabilities which can provide long durable thermoregulatory effect on the generated fibres. The extruded fibres can therefore be processed in a sustainable approach – avoiding the need of any organic solvents or high temperature for processibility.

3. Materials and methods

3.1. Materials

CNF suspensions in various solid contents were kindly provided by RISE Bio-economy (Sweden). The CNF suspension was produced from a softwood sulphite dissolving pulp (Domsjö Dissolving plus, Domsjö Fabriker AB, Sweden) by carboxymethylation (with sodium as a counterion) followed by fibrillation using a Microfluidizer M-110EH (Microfluidics Corporation, USA) at 1700 bar for 4 passes. The CNF had a charge density of -151 ± 2 μeq·g^{-1} at pH 5.2, measured using a particle charge detector PCD-02 (Mütek Analytic GmbH, Germany) based on titration with poly(diallyldimethylammonium) chloride. Cellulose nanocrystals (CNC) were procured from CelluForce, Canada. The morphology of CNC and CNF are represented in the AFM shown in Fig. S1 (supporting information). Hydrochloric acid (37 %), calcium chloride (98 %), paraffin wax (PW) with density of 0.82 g ml^{-1} at 20 °C were purchased from Sigma-Aldrich, Sweden. Fluorescence dye pyrene (98 %) was procured from Merck, Sweden. Nonionic fatty alcohol ethoxylate surfactant Ethylan 1008 was provided by Nouryon surface Chemistry, Stenungsund, Sweden.

3.2. Preparation of PCM microspheres

CNC was dispersed at 1 wt% in water by continuous stirring for 24 h and then sonication using a Vibracell sonicator (Sonics and Materials Inc., USA) for 10 min at 75 % amplitude. Paraffin wax in measured quantities was melted and then dispersed into aqueous suspension of CNC at 55 °C using a Heidolph DX900 high-speed homogenizer (Heidolph Instruments, equipped with a 10 mm shaft Germany) operating at 15,000 rpm for 2 min to form Pickering emulsion. The microspheres were characterized after cooling to room temperature.

3.3. Preparation of spinning dope

Different quantities of the PW dispersion were then dispersed into various concentrations of 10 ml CNF suspension at ambient temperature (ca. 23 °C) to form the spinning dope (see Table S1 for formulation details). The dope stability was assessed visually, and dope was deemed stable if no sedimentation was observed within 12 h. As the viscosity of the dope can affect the spinning behavior and the dispersibility of PW, CNF suspensions with concentration varying from 0.35, 0.5 to 0.75 wt% were tested.

3.4. Wet spinning

The CNF dopes with microspheres were extruded using a NE-1000 syringe pump (New Era Pump Systems Inc., USA) at a flow rate of 4.3 ml min^{-1} through a needle with an inner diameter of 275 μm into the coagulation bath containing 500 ml of hydrochloric acid (HCl) solution at pH 2. The coagulated wet fibres were collected on a winder drum rotating at a corresponding linear speed of 3 m min^{-1}. The winder was made from 6 pins located at a distance of 5 cm from each other and

outlining a circle, as reported previously (Nechyporchuk et al., 2017). This allowed drying the fibres in air without flattening. The fibres were dried at a temperature of 20 °C and a relative humidity of 65 % and detached afterward from the winder as separate fibres with the length of 50 mm.

3.5. Morphology of the spun fibres

The spun fibres were examined using a field emission scanning electron microscope (SEM) JSM-7800F (JEOL, Japan) coupled with an energy-dispersive X-ray spectroscopy analyzer. The samples were mounted on carbon tape and sputtered with Palladium (layer thickness of 4 nm). To prepare the cross sections, the fibres were frozen in liquid nitrogen and cut with a scalpel blade. The samples were analysed at an acceleration voltage of 10 kV at a working distance of 15 mm. Confocal images were captured using a Nikon Ti-E/A1+ high performance inverted confocal laser scanning microscope (excitation wavelength: 405 nm). Samples were thinly spread over a glass slide.

3.6. Electrophoresis

Zeta potential was measured using a Zeta PALS zeta potential analyzer from Brookhaven instrument corporation with a red He-Ne laser ($\lambda = 633$ nm). The PCM emulsions were diluted 10 times (*V*/V) from their starting concentrations with Milli-Q water and the average of 3 readings was reported. The data acquisition was done within a short time (10 s) for several cycles in order to prevent the effect of buoyancy forces.

3.7. Size of prepared microspheres

The average diameter of the solidified PCM droplets was measured by laser diffraction (Malvern MasterSizer Micro, Malvern Instruments Ltd.; Worcestershire, UK) the refractive index used was set to 1.421, and the measurement temperature was at 25 °C. The mean droplet size is based on the volume mean (D[4,3]) diameter. CNC-stabilized PCM emulsions were diluted 10 times with deionized water before analysing. Analyses were conducted in triplicate.

3.8. Thermal characterization

Thermal energy storage and release capacity of the microspheres were measured using a Mettler-Toledo 123 Differential Scanning Calorimeter (DSC). Sample were heated from 20 to 100 °C, held isothermal for 10 min at 100 °C, cooled from 100 to −80 °C and reheated again to 100 °C at a heating rate of 10 °C min^{-1} under nitrogen flow. The enthalpy of fusion from the second heating cycle was normalized to the actual content of PW in the sample. Thermal gravimetric analysis (TGA) was also performed on the same instrument. Samples were heated from 30 to 700 °C at the rate of 10 °C min^{-1} under nitrogen environment.

3.9. Washing fastness properties of spun fibres

Washing fastness assessment of the fibres was observed by subjecting the samples to a 1 wt% Ethylan 1008 nonionic surfactant solution at 50 °C for 15 min under constant stirring (the surfactant has a cloud point of 60 °C). Samples were then washed thoroughly with deionized water and dried at room temperature for 48 h. The change in dry weights before and after washing was used to determine the loss of paraffin wax from the samples. The process was repeated 10 times for the same set of samples and the average reading for 3 sets was used as the loss.

3.10. Thermal leak resistance properties of fibres

The leakage resistance of PW against subjection to heating and cooling was assessed by heating the fibres to 100 °C for 30 min on a glass slide, rubbing and tapping them off manually on the glass surface to get rid of excess wax which could have leached from the surface and quantifying the loss of weight after this. An average of three measurements was reported.

3.11. Tensile testing

The tensile properties of the fibres were measured using a Vibroskop (Lenzing AG, Austria) single fibre tensile tester. The fibres were conditioned and tested at a temperature of 20 °C and a relative humidity of 65 % (ISO 139:2005). The tensile testing was performed at a gauge length of 20 mm and a constant extension rate of 20 mm·min^{-1}. An average of 9 separate measurements is reported.

4. Results and discussion

4.1. Formulation and characterization of spinning dope

In the spinning dope formulation, the control of the size and stability of microsphere was of central importance. Typically, the PW particles size must be (i) smaller than the diameter of the nozzle to allow the extrusion of the dispersion into the coagulation media without clogging and (ii) smaller than the diameter of the resulting spun fibres, which otherwise will lead to fibres with largely deteriorated mechanical properties. To reach a microsphere dimension that allows incorporation into the fibres, two approaches have been compared, either using CNF or CNC as stabilizer.

The first approach consisted in directly dispersing the melted PW (10 wt% dry mass content) in a suspension of CNF, assuming that CNF would act as stabilizer at the oil/water interface (Capron et al., 2017; Varanasi et al., 2018). This was not the case, as evidenced by the presence of large lumps of PW right after the emulsification step (see Fig. 1a). Different concentrations of CNF, in the range 0.35–0.75 wt%, were tested and had no effect on the outcome.

In the second approach, CNC was used to prevent coalescence of PW droplets. Note that CNC has previously demonstrated a good ability in stabilizing oil-water interfaces, and has proven an excellent emulsification capacity, even with known hard-to-emulsify oils (Mikulcová et al., 2016). Molten PW was dispersed in 1 wt% aqueous suspension of CNC to yield a stable emulsion, see Fig. 1b and d, with average droplet size of 12 ± 4 μm, that could be cooled down to form microspheres without noticeable aggregation. CNC adsorption at the surface of the PW droplets was controlled by the wetting properties of the oil, as in conventional Pickering emulsions. The size of the droplet was in agreement with previous reports, and is mostly depending on the CNC concentration and emulsification conditions (Capron et al., 2017).

It was then possible to disperse these microspheres into the CNF suspensions at various concentrations to form suitable spinning dopes (Fig. 1c), as detailed in Table S1 (Supporting Information). The concentrations of CNF of 0.35, 0.5 and 0.75 wt% were examined to verify possible differences in dispersibility of CNC-stabilized PW within the fibre, along with spinnability efficacy and properties of the resulting fibres. PW content, with respect to the total dry mass of the spun fibre, was increased subsequently from 10 to 40 wt% in steps of 10 %, see Table 1. The aim here was to maximize the amount of PW in the dope which can then be processed into fibres. Above 40 wt% the stability of the dispersions was affected adversely. After dispersion of the microspheres into the CNF, the average PW size and electrophoretic mobility of the dope were measured, see Table 1. Size assessment and zeta potential values results from the presence of both CNF and PW and are reported here as a mean of stability of the spinning dope. The zeta potential values should be considered here as qualitative only, as the value obtained here results from the contribution of all the components. All the reported values were negative, as expected, yet to lower extent than pure CNC and CNF. The negative zeta potential values were deemed suitable for conducting a wet-spinning approach where the main fibre

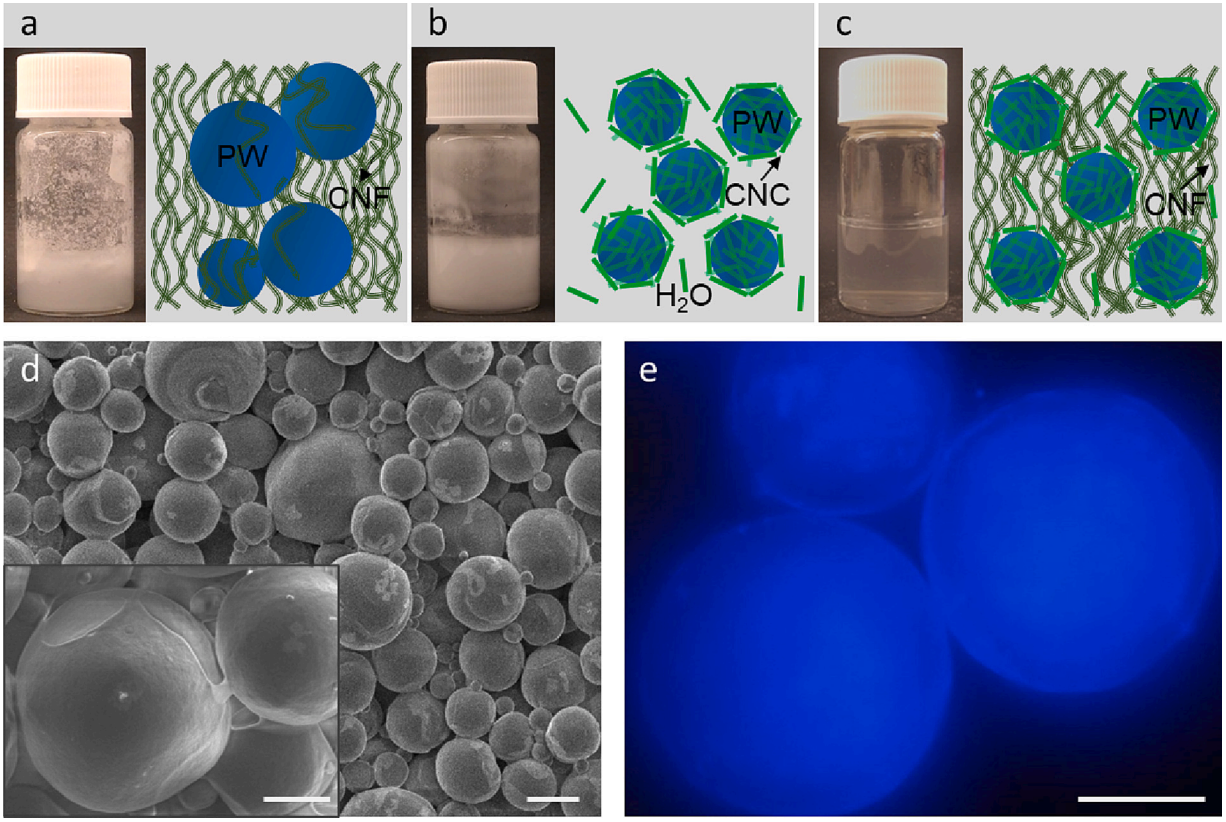

Fig. 1. a) Direct dispersion of PW (10 wt% with respect to cellulose) into 0.5 wt% CNF dispersion, b) PW stabilized with 1 wt% CNC with respect to the aqueous phase, volume fraction of PW is 0.05, volume fraction of aqueous phase is 0.95, c) dope produced from of an emulsion of PW stabilized by CNC, cooled and dispersed in CNF at 0.5 wt% to yield a 30 wt% PW with respect to CNF solids content, referred to as CNF35PW30, d) SEM images of CNC-stabilized PW microspheres, enlarged view is represented in the inset and e) confocal microscopy image of CNC stabilized PW microspheres where a fluorescent dye, namely pyrene, is incorporated into the wax phase, showing that wax is well contained in the core of the microspheres. White bars in (d), in the inset in (d) and in (e) represent a scale of 10 μm, 5 μm, and 5 μm, respectively.

Table 1
Formulation contents of PW and CNF along with diameter of microspheres and the resulting fibres. For reference, at 0.005 wt%, CNF and CNC had zeta potential values of -33.0 ± 0.5 mV and -30.0 ± 0.2 mV, respectively.

Sample name	Concentration of CNF stock suspension (wt%) (total of 10 g)	PW content in resultant CNF dry fibres (wt%)	Zeta potential (mV)	Diameter of microspheres (μm)	Diameter of fibres (μm)
CNF35P0	0.35	0	–	–	13 ± 3
CNF35PW10	0.35	10	-22 ± 0.4	10 ± 2	17 ± 3
CNF35PW20	0.35	20	-21 ± 0.5	10 ± 3	18 ± 4
CNF35PW30	0.35	30	-20 ± 0.5	11 ± 2	19 ± 2
CNF35PW40	0.35	40	-20 ± 0.7	12 ± 3	19 ± 3
CNF50P0	0.50	0	–	–	14 ± 2
CNF50PW10	0.5	10	-22 ± 0.3	9 ± 2	18 ± 3
CNF50PW20	0.5	20	-20 ± 0.5	10 ± 2	19 ± 2
CNF50PW30	0.5	30	-21 ± 0.4	10 ± 3	22 ± 4
CNF50PW40	0.5	40	-20 ± 0.2	12 ± 2	24 ± 3
CNF75P0	0.75	0	–	–	16 ± 2
CNF75PW10	0.75	10	-20 ± 0.6	10 ± 4	19 ± 2
CNF75PW20	0.75	20	-19 ± 0.3	11 ± 3	24 ± 4
CNF75PW30	0.75	30	-19 ± 0.5	12 ± 3	26 ± 3
CNF75PW40	0.75	40	-19 ± 0.4	12 ± 4	30 ± 2

formation mechanism is through controlled neutralization in the acidic conditions of the coagulation bath.

There was no significant difference in the PW size among the various formulations, supporting that the PW microspheres were quite stable and were resistant to aggregation, while no noticeable macroscopic phase separation could be observed.

The microspheres were further analysed by SEM which showed rather uniform microspheres. It can be seen that the oil droplets were covered by a layer of CNC. This was confirmed by fluorescence microscopy. A fluorescent dye was added to the wax phase before emulsification and the formed microspheres showed a bright core indicating the complete containment of PW inside the sheath of CNCs, as expected (Fig. 1e), without traces of oil leakage.

4.2. Spinning and characterization of the spun fibres

Wet spinning of the fibres was conducted using similar conditions that have proven to be effective with negatively charged CNF. The

coagulation of the CNF was induced by protonation of the anionic groups in acidic media (pH 2), resulting in formation of wet gel fibres, which were subsequently recovered from the coagulation bath and dried. Spinning trials with CNF concentration of 0.35, 0.50 and 0.75 wt %, referred to as CNF35, CNF50 and CNF75 respectively, were conducted while the content of paraffin wax was varied between 0 (e.g. CNF35P0) and 40 wt% on dry mass basis (e.g. CNF35P40). The process for fibre spinning is demonstrated in Figs. S2 and S3, as well as in video ESI 1.

All the fibres formed with this approach could be collected and allowed to dry under controlled conditions before further evaluation. The introduction of the PW microsphere did not hinder the process up to 40 wt%. Above this threshold, the CNF matrix formation was affected. Given that the microspheres have a diameter close to that of the fibres formed from CNF alone, this result could be anticipated. A potential increase of the PW content may be achieved by reducing the size of the microsphere. However, this approach was not evaluated.

The surface morphology of the fibres is presented in Fig. 2 and the corresponding average diameter is reported in Table 1. Fibres obtained from the dope containing pristine CNF had diameters of 13 ± 3, 14 ± 2 and 16 ± 2 μm, respectively, for the concentration mentioned above. The increase in CNF concentration led to increase in fibre diameter due to the higher solids content extruded per dope volume (Lundahl et al., 2017). Introduction of PW microsphere in the dope resulted in the formation of fibres with bulges likely originated from the dispersed domains of PW. The presence of these bulges gave rise to a surface roughness, which was more pronounced with increase in PW content against any given CNF concentration of the dope formulation. This was further validated with the SEM images of the cross-sections, as shown in Fig. 3. An increase in PW domains is observed by the presence of a greater number of bulges. The presence of the PW microsphere is clearly evidenced in panel (c) and (f) of the same figure and is further confirmed by the confocal microscopy images by the presence of dark microspheres as shown in Fig. 4. The PW domains are surrounded by the CNF nanofibres indicating their good encapsulation within the matrix of CNF.

These results indicate that it was possible to obtain PW encapsulated CNF fibres with a maximum of 40 wt% PW with respect to CNF content without affecting the continuity of the spinning. This could be attributed to the complete surface coverage of the PW droplets by CNC, which also bear anionic groups that can be protonated at pH 2, thus allowing the microsphere to coagulate in a similar fashion as CNF.

4.3. Thermal properties of the fibres

The thermal properties of the spun fibres were determined using DSC. Pristine paraffin wax was also analysed as a reference and showed a main melting peak at 55 °C and a minor peak at 35 °C, see Fig. 5a and b. Two crystallization peaks at 49 and 31 °C respectively, for the two corresponding melting peaks were observed. All the CNF/PW composites demonstrated characteristic temperatures, i.e., melting peaks at 55 ± 3 °C and 34 ± 3 °C and crystallization peaks at 49 ± 1 °C and 42 ± 3 °C, respectively, thus showing that the encapsulation had minor effect on the temperature of transition of the PW. The normalized enthalpies of fusion calculated for each system are reported in Table 2.

The intensity of the melting and crystallization peaks were found to be decreased in the composite fibres, however. This was particularly marked for the composite fibres with low PW contents. The normalized enthalpy of fusion and crystallization were also found to be reduced compared to 100 % PW sample which might be caused by the distribution of smaller isolated domains of PW dispersed in the matrix of CNF. The reduction in enthalpy of crystallization and fusion in isolated domains compared to bulk phase has been reported before (Andjelić & Scogna, 2015; Coupland, 2002; Michell et al., 2013). The normalized enthalpy of fusion and crystallization increased with increase in PW content, against constant CNF content. At any given CNF content in the dope, an addition of PW can obviously increase the content of PW in given volume of fibre and this can enhance their closeness and proximity in packing of PW as evident from the SEM and confocal microscopy images (Figs. 3 and 4). This resulted in formation of enhanced crystallization domains of PW yielding greater enthalpy of fusion and crystallization. This normalized enthalpy reduced with increase in CNF content against constant PW content which was linked directly to the PW content. An increase in CNF content in the dope is expected to increase the viscosity of the spinning dope. The PW microspheres dispersed in CNF matrix have a higher tendency to remain isolated from each at a higher CNF content, which can then result in lowering the enthalpy of fusion and crystallization of a given content of PW against increase in CNF concentration. This is illustrated in Fig. 6.

To validate the hypothesis of the influence of proximity of PW domains on the melting and crystallization enthalpy, neat CNF and PW were mixed in powder form in the same ratios as in the dope and were analysed by DSC. This is important, since, compared to simple mixtures of CNF and PW, the produced fibres with CNF matrix and CNC-stabilized PW have lower sizes of PW domains together with their better dispersion within CNF. It was found that, for a simple mixture, the enthalpy of

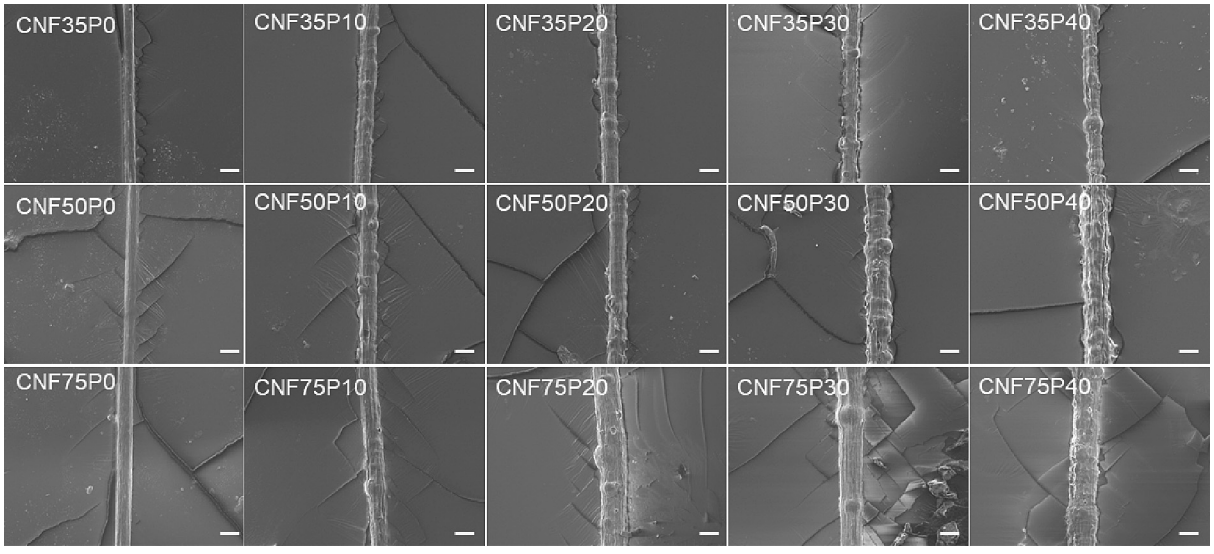

Fig. 2. Longitudinal view of surface morphology of the CNF-PW wet spun fibres. The white bar indicates a scale of 10 μm.

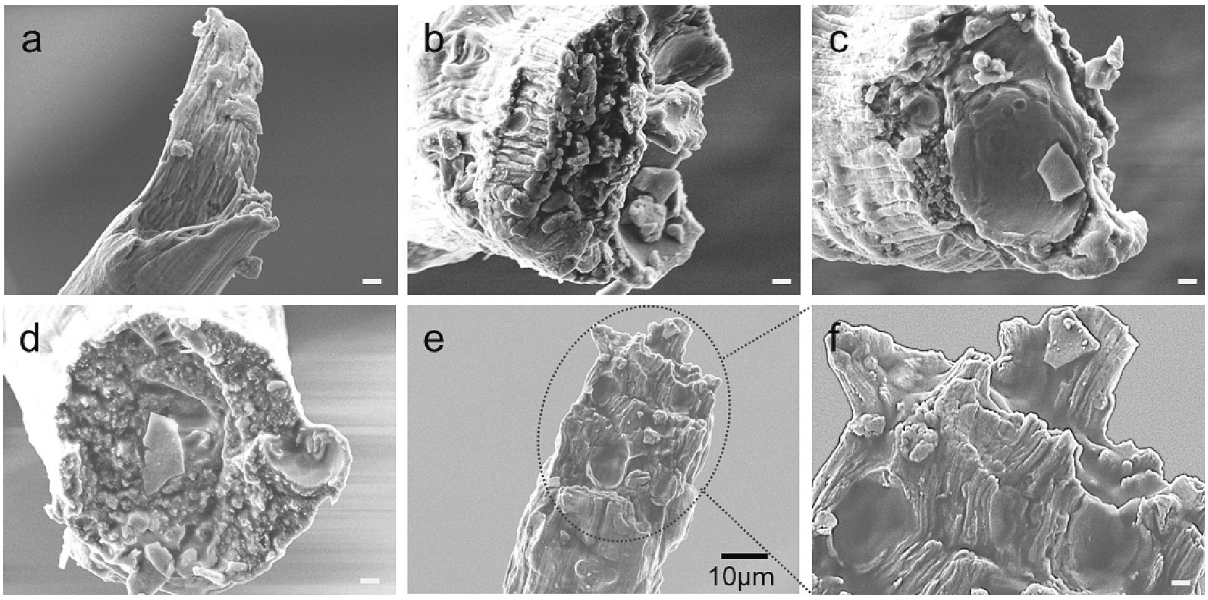

Fig. 3. Cross-section morphology of representative samples. a) pristine CNF35N b) CNF35P10 c) CNF35P20 d) CNF35P30, e) CNF35P40 and f) CNF35P40 magnified. The white bar indicates a scale of 1 μm unless otherwise indicated.

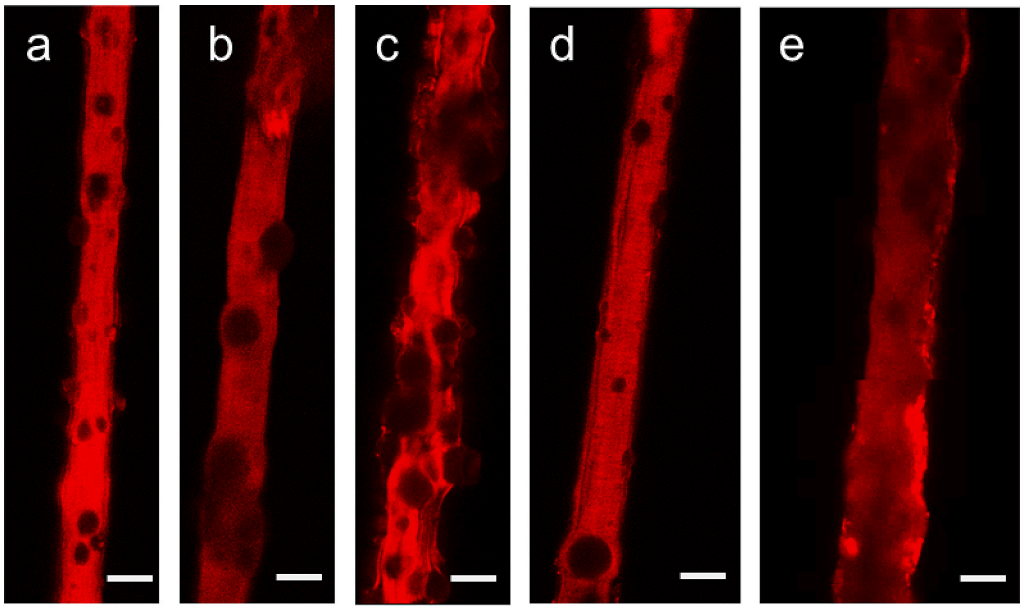

Fig. 4. Confocal images of CNF-PW samples indicating the proximity of PW domains across various samples. The PW in the fibres is indicated by the dark domains. a) CNF35P10, b) CNF35P20, c) CNF35P30, d) CNF50P10 and e) CNF75P10. The white bar indicates a scale of 20 μm. An increase in proximity of PW was observed with increase in PW content at constant CNF concentration. A reduction in proximity of PW domains was observed with increase in CNF concentration against constant PW content.

fusion and crystallization were much higher than in the fibrous matrix, i.e. 183 and 179 J g^{-1}, respectively, for 20 % PW-CNF dried mixture as compared to 64 and 63 J g^{-1}, respectively, for CNF35P20 fibres. Similarly, the melting and crystallization enthalpies were 229 and 228 J g^{-1}, respectively, for 30 % PW-CNF dried mixture as compared to 78 and 76 J g^{-1}, respectively, for the CNF35P30 sample. This shows that the proximity of PW domains along with their content in the resultant fibres affect the enthalpy of fusion and crystallization. The closer the PW domain, the better the PW crystals grow, which is hindered when they get isolated by CNF. The influence of the domain size on the lowering the crystallization enthalpy has been reported for other systems as well and underscores here the trade-off between domain size, distribution and stability (Qian et al., 2018).

The normalized melting and crystallization enthalpies of emulsion films made by casting the formulations with the same composition were compared against the corresponding enthalpies from the fibres, and are reported in Table 2. The crystallization and melting enthalpy of the casted films followed the same trend as that of fibres, i.e. an increase in both enthalpies with increase in PW content at constant CNF concentration and a lowering of enthalpies with increase in CNF concentration at constant PW content for the same reasons as suggested earlier. The crystallization and melting enthalpies were found to be lower against the enthalpies of the composite fibres at the same concentration of dope. Higher coalescence tendency of the PW during the passage through the spinneret while spinning might increase the proximity of the PW compared to segregated domains in the casted films. This can result in formation of continuous PW domains in the fibres, which results in higher crystallization enthalpies as compared to the isolated domains in films.

Thermal gravimetric analysis of the samples was performed to compare the onset of degradation temperature in the composite fibres, as shown in Fig. 5c. The degradation onset was similar to that of the

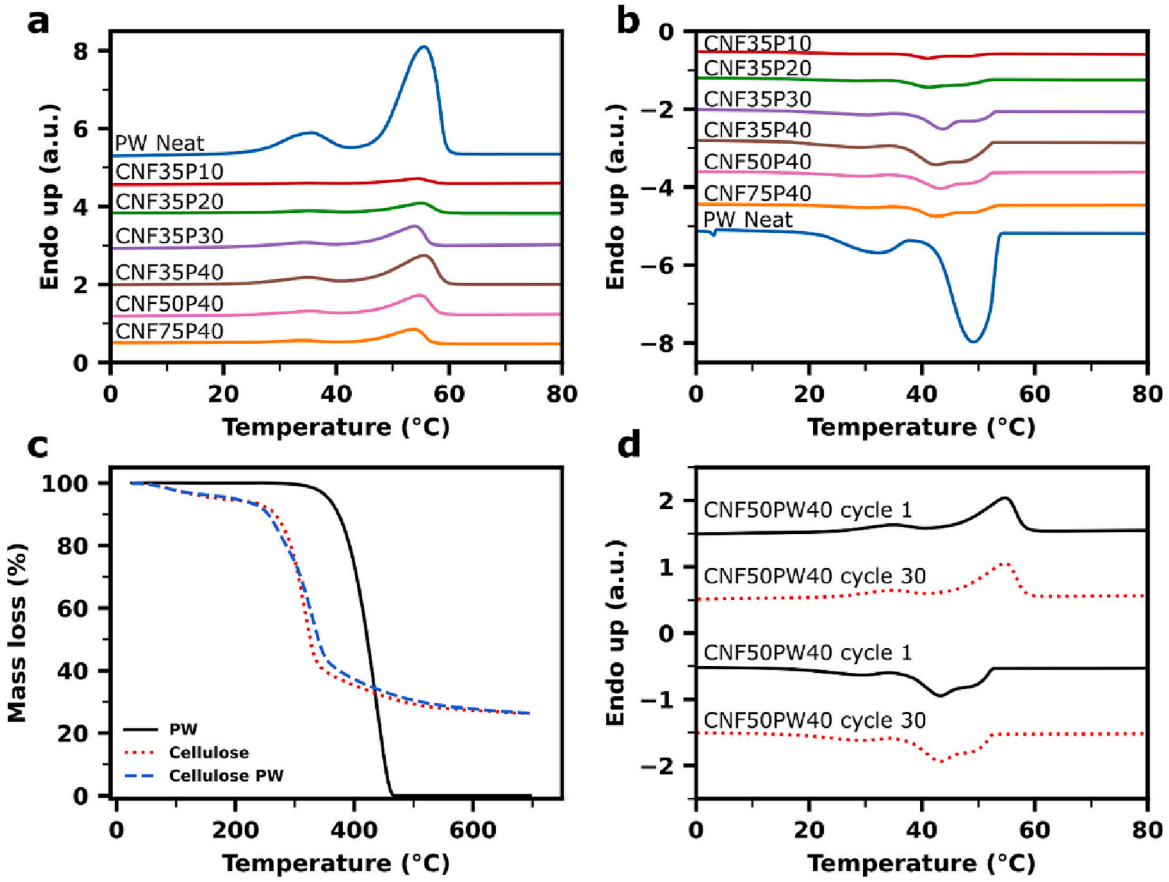

Fig. 5. DSC curves displaying fusion and crystallization of CNF-PW composite fibres. a) heating cycle b) cooling cycle c) TGA curve representing thermal degradation behavior of CNF, PW and their representative composites d) 1st and 30th heating-cooling cycle of the composite fibre CNF50PW40.

Table 2
Enthalpy of fusion and crystallization of CNF-PW fibres and films.

Sample name	Normalized enthalpy of fusion, cycle 2 (J g^{-1})	Normalized enthalpy of crystallization (J g^{-1})	Normalized enthalpy of fusion, cycle 2 (J g^{-1})	Normalized enthalpy of crystallization (J g^{-1})
	Fibres		Casted films	
Paraffin wax	147.39	147.30	–	–
CNF35PW10	61.05	54.71	39.60	26.70
CNF35PW20	63.95	62.95	43.70	41.95
CNF35PW30	78.33	76.67	56.87	55.40
CNF35PW40	99.17	94.63	59.83	59.65
CNF50PW10	50.30	41.01	9.60	8.20
CNF50PW20	53.23	52.30	10.15	10.30
CNF50PW30	55.33	53.27	12.43	12.93
CNF50PW40	60.4	57.53	15.73	15.53
CNF75PW10	31.5	25.4	1.10	1.00
CNF75PW20	35.7	33.9	1.35	1.20
CNF75PW30	41.27	39.2	1.87	1.40
CNF75PW40	43.78	42.63	2.40	2.03

pristine CNF fibres demonstrating that inclusion of 40 % PW in the samples does not affect the degradation properties compared to the control CNF fibres, signifying their potentials to be used as replacement to pristine CNF fibres. It also underscored that the PW did not promote the CNF degradation.

Further, endurance tests were conducted in the form of 30 repeated heating/cooling cycles of the fibres. The DSC curves of 30 phase change cycles of a representative sample CNF50P40 (Fig. 5d), fully coincide, and the phase change temperature and latent heat are identical in each melting - crystallizing cycle, indicating that the sample has a good cycle

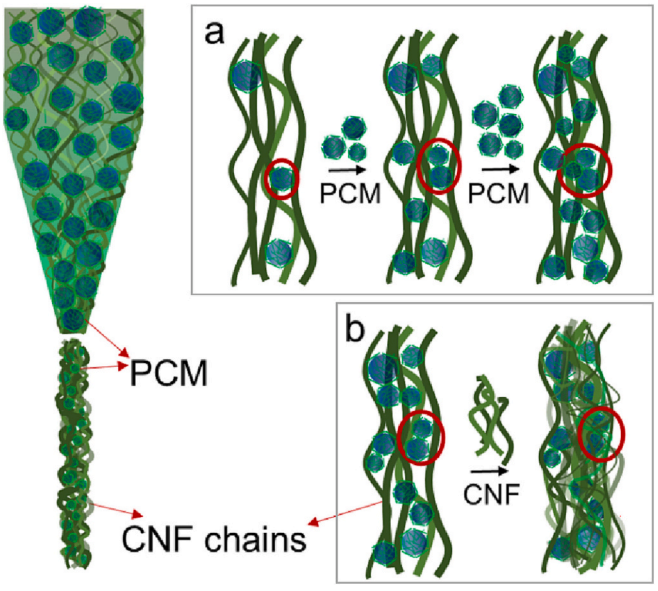

Fig. 6. Schematic representation of the proximity of PW domains with (a) increase in PW content at constant CNF concentration and (b) increase in CNF content at constant PW content in the spun fibres.

performance of phase transition.

4.4. Mechanical properties

The mechanical properties of the spun fibres were evaluated by tensile testing, and the composite fibres were compared to neat CNF fibres, shown in Fig. 7. The mechanical properties of the neat CNF fibres obtained here were comparable to the values reported in previous studies (Lundahl et al., 2016; Nechyporchuk et al., 2017; Vuoriluoto et al., 2017). The tenacity of the samples reduced slightly with an increase in CNF concentration in the dope, i.e., from 0.35 to 0.75 wt% of CNF. Lower CNF concentration was likely to result in dopes with lower crowding factor and viscosity that was believed to provide higher possibility for CNF alignment, which is in agreement with previous studies (Lundahl et al., 2016).

The incorporation of PW particles into the fibre bulk was expected to affect their mechanical properties, as it can disturb the continuity of CNF network along the fibre. Fig. 7 shows that the breaking tenacity of the fibres decreased gradually with an increase of the PW content in the fibre (see also Table S2 in the supporting information for the exact values). However, even at high PW content such as 40 wt%, it was still possible to reach a high breaking tenacity, e.g., 13.6 ± 1.5 cN tex^{-1} (ca. 135 MPa) for the sample spun based on 0.35 wt% CNF suspension. Furthermore, with the incorporation of PW, the elongation at break was found to increase. CNF chains are assumed to arrange themselves in regular ordered regions for forming crystallites. Inclusion of PW can disturb the alignment of the nanofibres resulting in random positioning of CNF surrounding the PW moieties. These CNF may undergo axial stretching during the mechanical testing. Furthermore, we also speculate that the presence of cellulose nanocrystals at the surface of the PW microsphere was beneficial to the mechanical properties in the sense that it enabled the CNF to be in contact with a cellulose-based interface instead of a hydrophobic interface with which it is poorly capable to interact, as demonstrated by the poor results of the emulsification tests.

4.5. Endurance tests of the fibres

Resistance and endurance of the fibres is a central feature in order to demonstrate the performance of the fibres for practical applications (Zhang et al., 2022). Repeated heating experiments, as well as exposure to detergent to mimic washing tests, were performed. The leak resistance properties of PW in CNF fibres were demonstrated by heating the samples to 100 °C for 30 min on a glass slide, rubbing and smearing them off manually over a glass surface to get rid of excess wax which could have leaked from the fibres, observing the structural differences under microscope and measuring the loss of weight. Representative samples of CNF35P40, CNF50P40 and CNF75P40 were analysed and a negligible loss of 0.2 ± 0.01, 0.7 ± 0.12 and 0.8 ± 0.04 wt%, respectively were observed after three times of such treatment. This demonstrated that the PW was well retained within the shell of CNC and the matrix of CNF which prevented its leakage even when exposed to 100 °C for several cycles. The treated samples were further analysed under DSC and the normalized enthalpy of fusion was 98, 59 and 42 J g^{-1}, whereas the enthalpy of crystallization was 93, 57 and 41 J g^{-1} for CNF35P40, CNF50P40 and CNF75P40, respectively. The values were quite close to the native fibres which were not exposed to endurance tests, (see Table 2) indicating good retainment of PW within the matrix of CNF, which can prevent its leakage at elevated temperatures of usage when the PW is in its molten state.

Good washing fastness of the composite fibres was also reported for fibres subjected to solution containing 1 wt% of a nonionic surfactant at 50 °C for 15 min under stirring. At this temperature the surfactant solution was close to its cloud temperature, at which the detergency is known maximal. Samples were washed thoroughly after this treatment with deionized water and dried at room temperature for 24 h. The process was repeated 10 times for the same set of samples and the average reading for 3 sets was recorded. The measured dry weight before and after washing suggested that the loss of paraffin wax from the samples was extremely small, i.e., samples CNF35P40, CNF50P40 and CNF75P40 showed a loss of mass of 1.0 ± 0.5, 1.0 ± 0.2 and 1.0 ± 0.4 wt%, respectively. This indicates that the samples are quite resilient to hot laundry cycles and display good retention of PW.

In addition, samples were immersed in toluene, a very good solvent for the PW, so as to conduct a solvent extraction. These samples were then analysed under SEM, as shown in Fig. 8. The representative solvent treated samples from CNF30P20 and CNF30P40 demonstrated retainment of the PCM domains as indicated by the yellow arrows. The enthalpy of fusion of these samples (3 replicates each) were measured after this solvent treatment process and the difference in normalized melting enthalpy was less than 1 %, which is within the standard deviation for the samples. This study therefore demonstrates the sturdy leak resistance properties of the prepared PCM encapsulated fibres evaluated and supported by different techniques.

5. Conclusion

This work reports on the development of thermo-regulating CNF fibres with incorporated CNC-stabilized PCM microspheres. The PCM used, a paraffin wax, was dispersed through a Pickering emulsion approach using CNC as stabilizer to form an interfacial layer of the same cellulosic nature as the CNF matrix of the spun fibre. The prepared microspheres were dispersed in CNF suspension to form stable and spinnable dope. We also showed that if PW was directly dispersed in the CNF matrix, the dope phase separated and was not spinnable.

The study of the thermal properties of the fibres revealed a clear correlation between the CNF concentration and the size and the dispersion of the microspheres. When using low concentration of CNF in the dope, the PW domains were larger and yielded higher enthalpies of

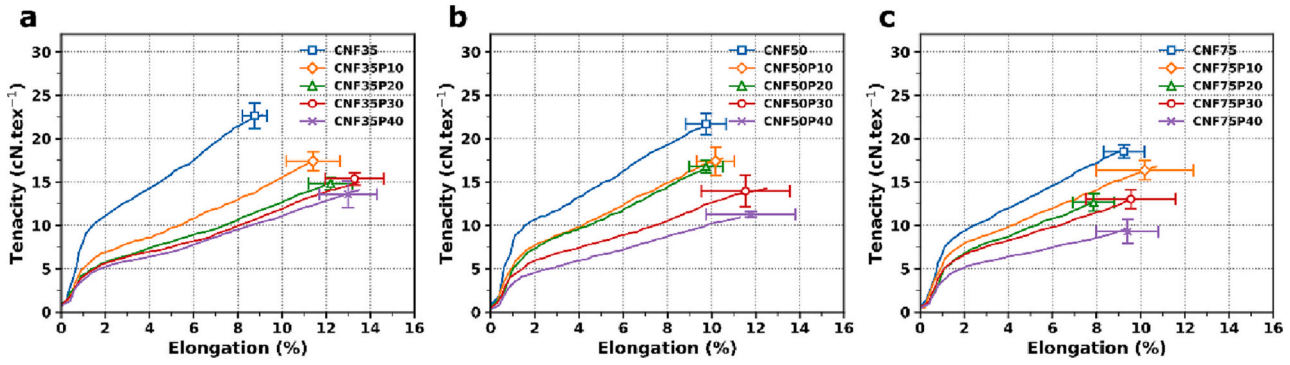

Fig. 7. Mechanical properties of the CNF-PW fibres a) pristine CNF and CNF-PW fibres at dope concentration of 0.35 wt% of CNF b) pristine CNF and CNF-PW fibres at dope concentration of 0.5 wt% of CNF c) pristine CNF and CNF-PW fibres at dope concentration of 0.5 wt% of CNF.

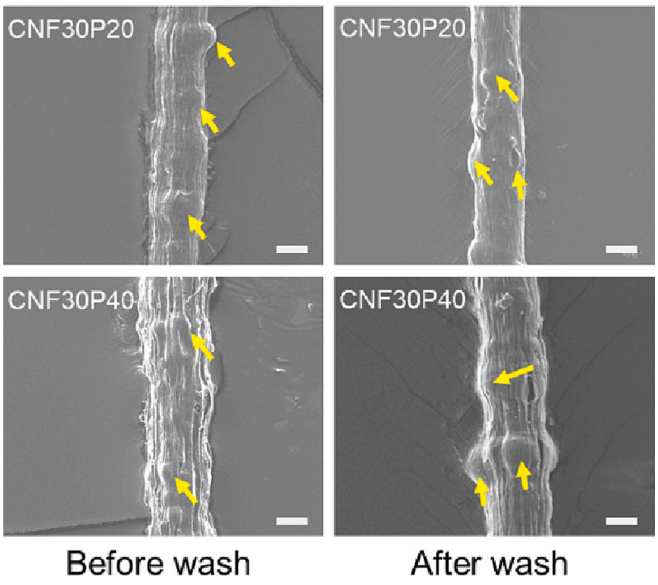

Fig. 8. Morphology of the fibres before and after extraction by toluene. The yellow arrows indicate retainment of PCM domains showcasing their leak resistance characteristics. The white bar indicates a scale of 10 μm. (For interpretation of the references to colour in this figure legend, the reader is referred to the web version of this article.)

fusion, implying a higher thermo-regulating capacity. Conversely, owing to a higher viscosity, higher CNF content limited the size of the PW domains, thus resulting in lower thermo-regulating capacity. It clearly illustrated that efficient thermo-regulating fibres, yet mechanically performing, can result in a trade-off that can be tuned with the PW content, with a benefit in using low CNF content.

At a high PCM content of 40 wt%, it was still possible to reach a high breaking tenacity, e.g., 13.6 ± 1.5 cN tex^{-1} (ca. 135 MPa) for the sample spun based on 0.35 wt% CNF suspension. The fibres also demonstrated good resistance against thermal leaching and showcased good wash fastness. Further optimization can be anticipated considering the amount of PW and their preferable localization in the fibre bulk or on the fibre surface. These aspects should be addressed for both good mechanical properties and efficient heat absorption. Additionally, the fibre mechanical properties may be further enhanced by applying drawing and other post-treatment operations.

Due to the renewable character of CNF, the developed fibres have a great potential for use in a wide range of applications. The most potential areas for future investigation are preparation of yarn that could then be weaved for textile application with emphasis on thermal properties evaluation of the biobased textiles.

Table showing formulation details for fabricating the microspheres and spinning dope, AFM images of CNF and CNC, schematic representing wet spinning system, photograph of the fibres during spinning and table showing mechanical properties of CNF-PW samples at various dope concentrations. Supplementary data to this article can be found online at https://doi.org/10.1016/j.carbpol.2023.120734.

Funding

This project has received funding from the VINNOVA, Sweden's innovation agency for financial support (grant # 2017-03724).

CRediT authorship contribution statement

Archana Samanta: Conceptualization, Investigation, Methodology, Data Curation, Writing. Oleksandr Nechyporchuk: Conceptualization, Investigation, Methodology, Data Curation, Writing. Romain Bordes: Conceptualization, Methodology, Writing. The manuscript was written through contributions of all authors. All authors have given approval to the final version of the manuscript.

Declaration of competing interest

The authors declare that they have no known competing financial interests or personal relationships that could have appeared to influence the work reported in this paper.

Data availability

Data will be made available on request.

Acknowledgement

This work was performed in part at the Chalmers Material Analysis Laboratory, CMAL.

References

Aftab, W., Huang, X., Wu, W., Liang, Z., Mahmood, A., & Zou, R. (2018). Nanoconfined phase change materials for thermal energy applications. *Energy & Environmental Science, 11*(6), 1392–1424. https://doi.org/10.1039/C7EE03587J

Andjelić, S., & Scogna, R. C. (2015). Polymer crystallization rate challenges: The art of chemistry and processing. *Journal of Applied Polymer Science, 132*(38), n/a-n/a. https://doi.org/10.1002/app.42066

Azizi Samir, M. A. S., Alloin, F., & Dufresne, A. (2005). Review of recent research into cellulosic whiskers, their properties and their application in nanocomposite field. *Biomacromolecules, 6*(2), 612–626. https://doi.org/10.1021/bm0493685

Bahsi Kaya, G., Kim, Y., Callahan, K., & Kundu, S. (2022). Microencapsulated phase change material via Pickering emulsion stabilized by cellulose nanofibrils for thermal energy storage. *Carbohydrate Polymers, 276*, Article 118745. https://doi.org/10.1016/j.carbpol.2021.118745

Barako, M. T., Lingamneni, S., Katz, J. S., Liu, T., Goodson, K. E., & Tice, J. (2018). Optimizing the design of composite phase change materials for high thermal power density. *Journal of Applied Physics, 124*(14), Article 145103. https://doi.org/10.1063/1.5031914

Bledzki, A. (1999). Composites reinforced with cellulose based fibres. *Progress in Polymer Science, 24*(2), 221–274. https://doi.org/10.1016/S0079-6700(98)00018-5

Capron, I., Rojas, O. J., & Bordes, R. (2017). Behavior of nanocelluloses at interfaces. *Current Opinion in Colloid & Interface Science, 29*, 83–95. https://doi.org/10.1016/j.cocis.2017.04.001

Cimilli Duru, S., Candan, C., & Uygun Nergis, B. (2019). Innovation in the comfort of intimate apparel. In F. Uddin (Ed.), *Textile Manufacturing Processes*. IntechOpen. https://doi.org/10.5772/intechopen.87115.

Clemons, C. (2016). Nanocellulose in spun continuous fibers: A review and future outlook. *Journal of Renewable Materials, 4*(5), 327–339. https://doi.org/10.7569/JRM.2016.634112

Coupland, J. N. (2002). Crystallization in emulsions. *Current Opinion in Colloid & Interface Science, 7*(5–6), 445–450. https://doi.org/10.1016/S1359-0294(02)00080-8

Cui, Y., Xie, J., Liu, J., Wang, J., & Chen, S. (2017). A review on phase change material application in building. *Advances in Mechanical Engineering, 9*(6). https://doi.org/10.1177/1687814017700828, 168781401770082.

Cunha, S., Aguiar, J., & Ferreira, V. (2016). Mortars with incorporation of phase change materials for thermal rehabilitation. *International Journal of Architectural Heritage, 1–10*. https://doi.org/10.1080/15583058.2016.1222464

Deveci, S. S., & Basal, G. (2009). Preparation of PCM microcapsules by complex coacervation of silk fibroin and chitosan. *Colloid and Polymer Science, 287*(12), 1455–1467. https://doi.org/10.1007/s00396-009-2115-z

Dhanabalan, S. C., Dhanabalan, B., Chen, X., Ponraj, J. S., & Zhang, H. (2019). Hybrid carbon nanostructured fibers: Stepping stone for intelligent textile-based electronics. *Nanoscale, 11*(7), 3046–3101. https://doi.org/10.1039/C8NR07554A

Ferreira, A. P., Childers, B., Melhem, R., Mosse, D., & Yousif, M. (2010). Using PCM in next-generation embedded space applications. In *2010 16th IEEE Real-Time and Embedded Technology and Applications Symposium* (pp. 153–162). https://doi.org/10.1109/RTAS.2010.40

Habibi, Y., Lucia, L. A., & Rojas, O. J. (2010). Cellulose nanocrystals: Chemistry, self-assembly, and applications. *Chemical Reviews, 110*(6), 3479–3500. https://doi.org/10.1021/cr900339w

Hooshmand, S., Aitomäki, Y., Norberg, N., Mathew, A. P., & Oksman, K. (2015). Dry-spun single-filament fibers comprising solely cellulose nanofibers from bioresidue. *ACS Applied Materials & Interfaces, 7*(23), 13022–13028. https://doi.org/10.1021/acsami.5b03091

Iqbal, K., Khan, A., Sun, D., Ashraf, M., Rehman, A., Safdar, F., Basit, A., & Maqsood, H. S. (2019). Phase change materials, their synthesis and application in textiles—A review. *The Journal of The Textile Institute, 110*(4), 625–638. https://doi.org/10.1080/00405000.2018.1548088

Iwamoto, S., Isogai, A., & Iwata, T. (2011). Structure and mechanical properties of wet-spun fibers made from natural cellulose nanofibers. *Biomacromolecules, 12*(3), 831–836. https://doi.org/10.1021/bm101510r

Li, M., Liu, J., & Shi, J. (2018). Synthesis and properties of phase change microcapsule with SiO2-TiO2 hybrid shell. *Solar Energy, 167*, 158–164. https://doi.org/10.1016/j.solener.2018.04.016

Li, Y., Yu, S., Chen, P., Rojas, R., Hajian, A., & Berglund, L. (2017). Cellulose nanofibers enable paraffin encapsulation and the formation of stable thermal regulation nanocomposites. *Nano Energy, 34*, 541–548. https://doi.org/10.1016/j.nanoen.2017.03.010

Ling, T.-C., & Poon, C.-S. (2013). Use of phase change materials for thermal energy storage in concrete: An overview. *Construction and Building Materials, 46*, 55–62. https://doi.org/10.1016/j.conbuildmat.2013.04.031

Lotnyk, A., Behrens, M., & Rauschenbach, B. (2019). Phase change thin films for non-volatile memory applications. *Nanoscale Advances, 1*(10), 3836–3857. https://doi.org/10.1039/C9NA00366E

Lundahl, M. J., Cunha, A. G., Rojo, E., Papageorgiou, A. C., Rautkari, L., Arboleda, J. C., & Rojas, O. J. (2016). Strength and water interactions of cellulose I filaments wet-spun from cellulose nanofibril hydrogels. *Scientific Reports, 6*(1), 30695. https://doi.org/10.1038/srep30695

Lundahl, M. J., Klar, V., Wang, L., Ago, M., & Rojas, O. J. (2017). Spinning of cellulose nanofibrils into filaments: A review. *Industrial & Engineering Chemistry Research, 56*(1), 8–19. https://doi.org/10.1021/acs.iecr.6b04010

McLaggan, M. S., Hadden, R. M., & Gillie, M. (2018). Fire performance of phase change material enhanced plasterboard. *Fire Technology, 54*(1), 117–134. https://doi.org/10.1007/s10694-017-0675-x

Meng, Q., Li, G., & Hu, J. (2015). Phase change fibers and assemblies. In X. Tao (Ed.), *Handbook of Smart Textiles* (pp. 225–251). Springer Singapore. https://doi.org/10.1007/978-981-4451-45-1_2.

Mertaniemi, H., Escobedo-Lucea, C., Sanz-Garcia, A., Gandía, C., Mäkitie, A., Partanen, J., Ikkala, O., & Yliperttula, M. (2016). Human stem cell decorated nanocellulose threads for biomedical applications. *Biomaterials, 82*, 208–220. https://doi.org/10.1016/j.biomaterials.2015.12.020

Michell, R. M., Blaszczyk-Lezak, I., Mijangos, C., & Müller, A. J. (2013). Confinement effects on polymer crystallization: From droplets to alumina nanopores. *Polymer, 54*(16), 4059–4077. https://doi.org/10.1016/j.polymer.2013.05.029

Mikulcová, V., Bordes, R., & Kašpárková, V. (2016). On the preparation and antibacterial activity of emulsions stabilized with nanocellulose particles. *Food Hydrocolloids, 61*, 780–792. https://doi.org/10.1016/j.foodhyd.2016.06.031

Mondal, S. (2008). Phase change materials for smart textiles – an overview. *Applied Thermal Engineering, 28*(11–12), 1536–1550. https://doi.org/10.1016/j.applthermaleng.2007.08.009

Nechyporchuk, O., Belgacem, M. N., & Bras, J. (2016). Production of cellulose nanofibrils: A review of recent advances. *Industrial Crops and Products, 93*, 2–25. https://doi.org/10.1016/j.indcrop.2016.02.016

Nechyporchuk, O., Bordes, R., & Köhnke, T. (2017). Wet spinning of flame-retardant cellulosic fibers supported by interfacial complexation of cellulose nanofibrils with silica nanoparticles. *ACS Applied Materials & Interfaces, 9*(44), 39069–39077. https://doi.org/10.1021/acsami.7b13466

Nechyporchuk, O., Håkansson, K. M. O., Gowda, V. K., Lundell, F., Hagström, B., & Köhnke, T. (2018). Continuous assembly of cellulose nanofibrils and nanocrystals into strong macrofibers through microfluidic spinning. *Advanced Materials Technologies*, 1800557. https://doi.org/10.1002/admt.201800557

Paulo, B. B., Andreola, K., Taranto, O., Ferreira, A. D., & Prata, A. S. (2019). Coating approach for a phase change material (PCM). *Powder Technology, 341*, 147–156. https://doi.org/10.1016/j.powtec.2018.03.003

Prajapati, D. G., & Kandasubramanian, B. (2019). A review on polymeric-based phase change material for thermo-regulating fabric application. *Polymer Reviews, 1–31*. https://doi.org/10.1080/15583724.2019.1677709

Qian, T., Li, J., Min, X., & Fan, B. (2018). Integration of pore confinement and hydrogen-bond influence on the crystallization behavior of C18 PCMs in mesoporous silica for form-stable phase change materials. *ACS Sustainable Chemistry & Engineering, 6*(1), 897–908. https://doi.org/10.1021/acssuschemeng.7b03267

Revaiah, R. G., Kotresh, T. M., & Kandasubramanian, B. (2019). Technical textiles for military applications. *The Journal of The Textile Institute, 1–36*. https://doi.org/10.1080/00405000.2019.1627987

Saito, T., Kuramae, R., Wohlert, J., Berglund, L. A., & Isogai, A. (2013). An ultrastrong nanofibrillar biomaterial: The strength of single cellulose nanofibrils revealed via sonication-induced fragmentation. *Biomacromolecules, 14*(1), 248–253. https://doi.org/10.1021/bm301674e

Sarier, N., Onder, E., & Ukuser, G. (2015). Silver incorporated microencapsulation of n-hexadecane and n-octadecane appropriate for dynamic thermal management in textiles. *Thermochimica Acta, 613*, 17–27. https://doi.org/10.1016/j.tca.2015.05.015

Sharma, A., Tyagi, V. V., Chen, C. R., & Buddhi, D. (2009). Review on thermal energy storage with phase change materials and applications. *Renewable and Sustainable Energy Reviews, 13*(2), 318–345. https://doi.org/10.1016/j.rser.2007.10.005

Shen, Y., Orelma, H., Sneck, A., Kataja, K., Salmela, J., Qvintus, P., Suurnäkki, A., & Harlin, A. (2016). High velocity dry spinning of nanofibrillated cellulose (CNF) filaments on an adhesion controlled surface with low friction. *Cellulose, 23*(6), 3393–3398. https://doi.org/10.1007/s10570-016-1044-5

Shi, X., Yazdani, M. R., Ajdary, R., & Rojas, O. J. (2021). Leakage-proof microencapsulation of phase change materials by emulsification with acetylated cellulose nanofibrils. *Carbohydrate Polymers, 254*, Article 117279. https://doi.org/10.1016/j.carbpol.2020.117279

Singh, S., Gaikwad, K. K., & Lee, Y. S. (2018). Phase change materials for advanced cooling packaging. *Environmental Chemistry Letters, 16*(3), 845–859. https://doi.org/10.1007/s10311-018-0726-7

Siró, I., & Plackett, D. (2010). Microfibrillated cellulose and new nanocomposite materials: A review. *Cellulose, 17*(3), 459–494. https://doi.org/10.1007/s10570-010-9405-y

Song, M., Jiang, J., Zhu, J., Zheng, Y., Yu, Z., Ren, X., & Jiang, F. (2021). Lightweight, strong, and form-stable cellulose nanofibrils phase change aerogel with high latent heat. *Carbohydrate Polymers, 272*, Article 118460. https://doi.org/10.1016/j.carbpol.2021.118460

Varanasi, S., Henzel, L., Mendoza, L., Prathapan, R., Batchelor, W., Tabor, R., & Garnier, G. (2018). Pickering emulsions electrostatically stabilized by cellulose nanocrystals. *Frontiers in Chemistry, 6*, 409. https://doi.org/10.3389/fchem.2018.00409

Vuoriluoto, M., Orelma, H., Lundahl, M., Borghei, M., & Rojas, O. J. (2017). Filaments with affinity binding and wet strength can be achieved by spinning bifunctional cellulose nanofibrils. *Biomacromolecules, 18*(6), 1803–1813. https://doi.org/10.1021/acs.biomac.7b00256

Walther, A., Timonen, J. V. I., Díez, I., Laukkanen, A., & Ikkala, O. (2011). Multifunctional high-performance biofibers based on wet-extrusion of renewable native cellulose nanofibrils. *Advanced Materials, 23*(26), 2924–2928. https://doi.org/10.1002/adma.201100580

Wei, J., Li, Z., Liu, L., & Liu, X. (2013). Preparation and characterization of novel polyamide paraffin MEPCM by interfacial polymerization technique. *Journal of Applied Polymer Science, 127*(6), 4588–4593. https://doi.org/10.1002/app.37681

Yang, B., Fu, X., Yang, W., Sun, N., Hu, S., Lu, Y., & Yang, M.-B. (2010). Prediction of heat conduction with phase-change effects during cooling stage of injection molding of high-density polyethylene: Approximate integral approach. *Journal of Macromolecular Science, Part B, 49*(4), 734–749. https://doi.org/10.1080/00222341003600780

Yu, S., Wang, X., & Wu, D. (2014). Microencapsulation of n-octadecane phase change material with calcium carbonate shell for enhancement of thermal conductivity and serving durability: Synthesis, microstructure, and performance evaluation. *Applied Energy, 114*, 632–643. https://doi.org/10.1016/j.apenergy.2013.10.029

Zhang, J., Xu, Y., Li, X., Li, H., Yao, C., Chen, S., & Xu, F. (2022). Leak-free, high latent heat and self-cleaning phase change materials supported by layered cellulose/Fe3O4 skeleton for light-to-thermal energy conversion. *Energy Conversion and Management, 256*, Article 115357. https://doi.org/10.1016/j.enconman.2022.115357

Zhang, Y., Li, Y., Ma, H., & Yu, T. (2013). Tensile and interfacial properties of unidirectional flax/glass fiber reinforced hybrid composites. *Composites Science and Technology, 88*, 172–177. https://doi.org/10.1016/j.compscitech.2013.08.037

Zhao, M., Zhang, X., & Kong, X. (2020). Preparation and characterization of a novel composite phase change material with double phase change points based on nanocapsules. *Renewable Energy, 147*, 374–383. https://doi.org/10.1016/j.renene.2019.08.117

Zheng, Y., Oguzlu, H., Baldelli, A., Zhu, Y., Song, M., Pratap-Singh, A., & Jiang, F. (2022). Sprayable cellulose nanofibrils stabilized phase change material Pickering emulsion for spray coating application. *Carbohydrate Polymers, 291*, Article 119583. https://doi.org/10.1016/j.carbpol.2022.119583

Zhou, D., Zhao, C. Y., & Tian, Y. (2012). Review on thermal energy storage with phase change materials (PCMs) in building applications. *Applied Energy, 92*, 593–605. https://doi.org/10.1016/j.apenergy.2011.08.025

Zhou, T., Darkwa, J., & Kokogiannakis, G. (2015). Thermal evaluation of laminated composite phase change material gypsum board under dynamic conditions. *Renewable Energy, 78*, 448–456. https://doi.org/10.1016/j.renene.2015.01.025